Published in final edited form as:

Comput Methods Programs Biomed. 2022 June ; 221: 106890. doi:10.1016/j.cmpb.2022.106890.

Digitizing ECG image: a new method and open-source software code

Julian D. Fortune, HBS[1], **Natalie E. Coppa**[1], **Kazi T. Haq, Ph.D**[2], **Hetal Patel, BS, MS**[2,3], **Larisa G. Tereshchenko, M.D, Ph.D**[2,4]

[1]Oregon State University, Corvallis, OR

[2]Oregon Health & Science University, Knight Cardiovascular Institute, Portland, OR

[3]Chicago Medical School at Rosalind Franklin University, IL

[4]Cleveland Clinic Lerner Research Institute, Department of Quantitative Health Sciences, Cleveland, OH

Abstract

Background and Objective: We aimed to develop and validate an open-source code ECG-digitizing tool and assess agreements of ECG measurements across three types of median beats, comprised of digitally recorded simultaneous and asynchronous ECG leads and digitized asynchronous ECG leads.

Methods: We used the data of clinical studies participants (n=230; mean age 30±15 y; 25% female; 52% had the cardiovascular disease) with available both digitally recorded and printed on paper and then scanned ECGs, split into development (n=150) and validation (n=80) datasets. The agreement between ECG and VCG measurements on the digitally recorded time-coherent median beat, representative asynchronous digitized, and digitally recorded beats was assessed by Bland-Altman analysis.

Results: The sample-per-sample comparison of digitally recorded and digitized signals showed a very high correlation (0.977), a small mean difference (9.3 μV), and root mean squared error (25.9 μV). Agreement between digitally recorded and digitized representative beat was high [area spatial ventricular gradient (SVG) elevation bias 2.5(95% limits of agreement [LOA] −7.9-13.0)°; precision 96.8%; inter-class correlation [ICC] 0.988; Lin's concordance coefficient ρ_c 0.97(95% confidence interval [CI] 0.95-0.98)]. Agreement between digitally recorded asynchronous and time-coherent median beats was moderate for area-based VCG metrics (spatial QRS-T angle bias 1.4(95%LOA −33.2-30.3)°; precision 94.8%; ICC 0.95; Lin's concordance coefficient ρ_c 0.90(95%CI 0.82-0.95)].

Conclusions: We developed and validated an open-source software tool for paper-ECG digitization. Asynchronous ECG leads are the primary source of disagreement in measurements on digitally recorded and digitized ECGs.

Correspondence: Larisa Tereshchenko, 9500 Euclid Ave, JJN3-01. Cleveland, OH, 44195. tereshl@ccf.org.

Keywords

ECG; digitization; paper-to-digital conversion; paper ECG digitizing; ECG paper digital conversion

Introduction

An electrocardiogram (ECG) is a ubiquitous, inexpensive, and noninvasive diagnostic tool. The ECG is widely used in everyday clinical practice around the globe. Traditionally, clinical ECG analyses was conducted on paper ECG printouts, either directly or using magnifying on-screen calipers. There are many manufacturers of ECG recording equipment. Each manufacturing company saves ECG data in a proprietary, encrypted file format. Despite substantial efforts and undeniable progress,[1] open digital ECG data files from various ECG manufacturers are not easily available for clinicians due to the lack of compatibility of the data across different systems. Furthermore, legacy Electronic Medical Record (EMR) systems require printed ECG images for clinical ECG analysis. Therefore, despite the existence of digital ECG technologies, clinicians continue to collect paper ECG images (but not digital ECG files) of clinically important ECGs, illustrating the importance of an ECG for diagnosis and patient management.

For example, the Food and Drug Administration (FDA) must verify the safety of all new drugs coming to the U.S. market, which requires assessment of the QT-prolonging effect of new drugs. To standardize the submission of the ECG data to the FDA for systematic evaluation, the FDA championed the digital ECG initiative. In response, an American National Standards Institute – accredited the Health Level Seven International (HL7) organization developed an annotated ECG standard.[2] The FDA's digital ECG initiative facilitated the development and widespread use of paper ECG digitizing tools. [3] This enabled the use of paper ECG records collected by pharmaceutical companies during randomized clinical trials, which did not plan to collect digital ECG files, despite existing digital ECG technologies.

Besides clinical practice, the ECG is a common phenotype used in population-based prospective cohorts, "big data" genomics[4], and artificial intelligence (AI) studies.[5] Notably, an ECG characterizes the electrophysiological substrate of cardiovascular diseases and can be easily recorded in hundreds of thousands of people. Thus, ECG data provides the statistical power for analyses of rare clinical outcomes (e.g. sudden cardiac death) that require a large sample size and long term follow up. [6] Nowadays, an ECG is routinely saved and stored as a digital file. However, until the end of the 20th century, the ECG was recorded only on paper. Many large-scale longitudinal clinical studies that were conducted in the 20th century collected thousands of unique paper-printed ECGs (e.g., Coronary Artery Risk Development in Young Adults (CARDIA), Multiple Risk Factor Intervention Trial (MRFIT), Reasons for Geographic and Racial Differences in Stroke Study (REGARDS), the Antihypertensive and Lipid-Lowering Treatment to Prevent Heart Attack Trial (ALLHAT), to name just a few.[7] National Institute of Health advocated for paper ECG digitization for many years.[8] Paper-printed ECGs must be scanned and digitized to make them available

for future AI studies[9] and the application of novel analytical approaches, such as global electrical heterogeneity (GEH) measurement.[6] Some examples of large-scale clinical studies with successful paper ECG digitizing include Mini-Finland Health Survey,[10] the SmartDelay Determined Atrioventricular (AV) Optimization (SMART-AV) randomized controlled trial,[11] and others.[12]

Furthermore, there have been successful attempts to discriminate between normal sinus rhythm and atrial fibrillation using deep neural network analysis of ambulatory paper ECG images.[9] Brisk et al. argued that even without perfectly accurate ECG digitization, deep learning of paper ECG images could be useful for the detection of cardiac arrhythmia.[9] Both approaches (paper ECG digitization and deep learning of paper ECG images) require detection of an ECG signal and discrimination between the ECG signal and the paper grid. A renewed interest in paper ECG digitization is facilitated by easily available EMR ECG images and their independence of recording separate from the ECG equipment manufacturer.

Several ECG-digitizing tools have been previously developed.[7] The most widely used is the ECGScan, a patented commercially available computer application.[3] The ECGScan utilized the concept of active contours and dynamic programming providing the possibility for the user to set anchor points on the ECG waveform's image manually. While the users usually appreciated the possibility to provide their input, manual "correction" of the ECG waveform was time-consuming and reduced the reproducibility of the ECG digitization.[3, 13] Previously, there was no open-source code ECG-digitizing tool available.

It is well-recognized that the digitized ECG is inferior to the digitally recorded ECG.[3, 7, 13] Compared to the digitally recorded ECG, the digitized ECG inevitably loses the information and should be used only if a digitally recorded ECG is not available.[8] Of note, historic ECG machines and the standard 3x4 display of a 12-lead ECG printout show different ECG leads over time. However, current standards require ECG measurements to be performed on a median beat that are created from simultaneously recorded ECG leads.[14] Such requirements cannot be fulfilled using asynchronous digitized ECG leads. Notably, vectorcardiogram (VCG) analysis requires transformation of eight simultaneously recorded ECG leads into orthogonal XYZ leads. However, the degree of agreement between ECG measurements performed on a median beat comprised of simultaneously versus asynchronously recorded ECG leads has not been assessed.

Recent advancements in AI algorithms opened avenues for further development of ECG-digitizing tools. In the present study, we aimed to develop and validate an open-source code ECG-digitizing tool and assess agreements of the standard ECG and VCG GEH measurements across 3 types of median or representative beats comprised of (1) digitally recorded, simultaneous ECG leads, (2) digitally recorded, asynchronous ECG leads, and (3) digitized, asynchronous ECG leads.

Methods

1.1. Study population and ECG recording

For the development and validation of the algorithm, we used the data of clinical studies conducted at the Oregon Health & Science University (OHSU), with available both (1) digitally recorded ECGs and (2) printed on paper ECGs.[15–18] All studies were approved by the OHSU Institutional Review Board, and all participants signed informed consent before entering the study. In the present study, we excluded participants with atrial fibrillation or flutter recorded on a 12-lead ECG. All participants were in sinus rhythm.

Routine resting 10-second 12-lead ECGs were recorded using a MAC 5500 HD ECG system (General Electric (GE) Healthcare Technologies, Marquette Electronics, Milwaukee, WI). The ECGs were printed with a standard output mode: at the paper speed of 25 mm/s and 10 mm/mV calibration, in a 3x4 display mode. Consecutive 2.5 seconds were displayed on a printed ECG record so that the first 2.5 seconds displayed leads I, II, III, the second 2.5 seconds displayed leads aVR, aVL, aVF, the third 2.5 seconds displayed leads V1, V2, V3, and the final 2.5 seconds displayed leads V4, V5, and V6.

Paper ECG printouts were scanned at 600 dpi resolution, auto-color mode, scan speed up to 160 opm, TIFF output file format, using Konica Minolta Bizhub 284E (Konica Minolta, Tokyo, Japan). We used the Magellan ECG Research Workstation V2 (GE Marquette Electronics, Milwaukee, WI) to obtain the raw digital ECG signal with the sampling rate of 500 samples/sec and 1 μV amplitude resolution.

1.2. Algorithm development and description

2.2.1. Algorithm overview—The algorithm and open-source software code, written in Python (Python Software Foundation, Delaware, US), are provided at https://github.com/Tereshchenkolab/paper-ecg. Figure 1 shows the overview flowchart of the developed algorithm. The complex task of digitizing a scan containing many ECG leads was subdivided into 3 steps to clarify the scope (pre-processing, detection, and extraction; Table 1).

The digitization process involves two processes, grid digitization and signal digitization (Figure 2). The detection involves converting a color image of a cropped ECG lead into a binary image such that only pixels of interest are *True*. The extraction takes the binary image as an input and generates the relevant output: a scalar estimate of the spacing for the grid and an array of height values for the signal.

2.2.2. Image pre-processing. Graphical User Interface.—First, the application prepares the ECG scan, allows rotation/normalization, crops individual ECG leads, and integrates the digitized data from all leads (Figure 3). The inputs consist of the color image of the scanned ECG and user inputs for rotation, lead locations, lead start time, and grid scale. If needed, the user can manually rotate the image, using the slider on the control panel. The input image is cropped based on the user inputs to produce between one and twelve images of individual leads. Each of these lead images goes through the same digitization process, and the digitization outputs are all joined together into a matrix which

is outputted to a file. A Graphical User Interface (GUI) is described in the Supplement (Supplemental Figures 1–2). Figure 4 depicts the typical user workflow when using the application.

2.2.3. Grid detection—The robust nature of the grid extraction method allows for a simplistic, and therefore efficient, threshold process: the image is converted to grayscale, the white point is normalized using the median intensity, and a static threshold is used to generate a binary image. The grayscale conversion is performed by the OpenCV implementation *(cvtColor())*, which calculates the intensity (luminance value *I)*, or "gray" value for each pixel, as shown in equation 1, where p_r is the pixel's red value, p_g is the pixel's green value, p_b is the pixel's blue value.[19]

$$I = 0.299 \times p_r + 0.587 \times p_g + 0.114 \times p_b \quad \text{(eq 1)}$$

[20]

Next, the histogram of the grayscale image is computed, and the median of the histogram is assumed to be a representative value for white. Then, the pixels' values are multiplied (element-wise) by the median value of the histogram divided by 255 to create a white-point-adjusted image. Lastly, all pixels with intensities above 230 are marked as *True* in a binary version of the input image, and all other pixels are marked *False*. The binary image can be interpreted as a *mask* that isolates the grid part of the image. The threshold value, 230, was chosen based on manual tuning on a subset of cropped ECG lead images from various scans used to verify the code was performing as expected (referred to as the "Development dataset").

2.2.4. Grid extraction—The grid extraction is performed in both horizontal and vertical directions separately through a special autocorrelation. A density signal is produced by summing the *True* pixels in a row or column across the whole image. Both the horizontal and vertical density signals are computed to estimate the grid spacing in each direction (Figure 5). The fundamental period (the period of the fundamental frequency) of the horizontal and vertical density signals is obtained via computing the autocorrelation and selecting the first peak in the autocorrelation signal with a height greater than 0.3 (the range of autocorrelation is [−1, 1]) and prominence of 0.05 implemented via the SciPy library.[21] These parameters were chosen via manual tuning using the development dataset. A step size of one pixel is used for autocorrelation, and this may result in a large error when the grid size is on the order of one or ten pixels. Therefore, a quadratic function is fitted to the two adjacent points around the peak and the peak itself (three points total), and the maximum over that function (with a precision of 0.01 pixels) is taken as the true period of the grid. The correlation and prominence thresholds are heuristic and have been selected by testing a range of values in the development dataset to ensure the best performance for all ECG images in the development dataset.

The pixel-counting approach to grid extraction is robust to slight changes in rotation but may suffer when the rotation is sufficiently erroneous. When multiple horizontal grid lines are counted in the same row of the image or multiple vertical grid lines are counted in

the same column of the image, the signal will not have sharp peaks, which can cause fundamental period analysis to fail in finding an acceptable peak. The row analysis is more sensitive because it involves long lines, which increases the likelihood of overlap and, in turn, diminishes peaks in the count signal. Therefore, the output from grid extraction is the period estimate from the columns when available, and the period estimate from the rows only when the column estimation fails.

2.2.5. Signal detection—The signal detection relies upon the grid extraction module to detect when a grid is or is not present in order to adaptively set the threshold. The process begins by converting the image to grayscale using equation 3, selecting a starting threshold based on Otsu's method,[22] and creating a binary image based on that threshold. Next, iteratively, grid extraction is applied. If grid extractions succeed (i.e., an estimate for the spacing is returned), this threshold is reduced by 5%, and a new binary image is created. The iteration stops when the reduced threshold is below 60% of the original threshold or grid extraction fails (i.e., the grid is not sufficiently salient in the binary image). The stopping point of 60% was chosen based on the development dataset. The step size of 5% was chosen to balance run-time with sufficient granularity, which was verified on the Development dataset. The final binary image created during the linear search is returned.

2.2.6. Signal Extraction—The signal extraction algorithm is based on the Viterbi dynamic programming (DP) algorithm,[23] where contiguous regions in each column of the image are treated as nodes, and a custom score (cost) function is used to select the most likely path for the signal. The first step involves examining each column or horizontal slice of the input binary image and marking the center of each region of contiguous *True* pixels. This produces a list of lists of points in each column that are sorted topologically when scanning across the image from left to right.

Next, a so-called DP table is built that stores the best path and the associated score for that best path for each node. First, all the points in the first column of the image are stored in the DP table as base cases with costs of zero. Then, the points in each column are processed starting with the second column from the left and going to the rightmost column. At each point, possible connections can be made to candidate points in the nearest prior column containing points. This is typically the immediately-prior column, but columns can be empty. Each possible connection has a total cost consisting of the cost to get to the candidate point plus the cost to transition from the candidate point to the current point. The cost function C is defined in equation 2,[24]

$$C(p_1, p_2, a) = D(p_1, p_2) \times \alpha + S(a, \angle(p_1, p_2)) \times (1 - \alpha) \quad \text{(eq 2)}$$

[24], where: p_1 is the candidate point, p_2 is the current point, a is the angle ($\angle$) of the connection arriving at the candidate point (i.e., the instantaneous direction of the path at p_1), D (*distance)* returns the Euclidean distance between two points, α *(alpha)* is a parameter to control the relative weight of distance and angle alignment, the *similarity* S is defined in equation 3, and $\angle$ (*angle)* is the angle between two points in degrees.

$$S(a_1, a_2) = \frac{(180 - |a_1 - a_2|)}{180} \quad \text{(eq 3)}$$

[24].

The candidate point with the minimal total cost is selected as the best path to the current point, and this is recorded in the DP table. If no possible connections can be found, the point becomes a base case with a cost of zero. The cost function is designed to grant a lower cost for points that are closer in the image and penalize points that are distant because the shape of the signal is generally continuous (i.e., does not involve abrupt jumps up or down from one instant to the next) and does not involve large horizontal gaps. The costs function also penalizes large changes in direction by comparing the change in direction from one point to the next because the line is generally relatively smooth. The value of *alpha* 0.5 is selected, as determined by manual examination on the development dataset.

An example of a DP table is shown in Figure 6, where blue represents a low total cost and maroon a high total cost. Once the DP table has been constructed for all points in the image, a single best path is chosen by searching for the path with the lowest cost in the last 20 columns in the image. Then, backtracking is performed by following the back-references in the entry for each point in the DP table to construct the entire path. There is a final step to convert the list of points to an array of the y values that linearly interpolates between columns where points are absent, and this array is returned.

2.2.7. Post-processing—The integration process takes the un-altered signal (i.e., pixel height locations for every column in the image) and grid sizing from the digitization module for each lead the user has elected to digitize and creates a matrix with a column for each lead to output to a file. The grid spacings from all leads where grid digitization was successful are averaged to get a more robust estimate and provide an estimate in cases where grid digitization failed for a lead image. Then, the same post-processing is applied to the outputs from the digitization process for all leads.

The first step of post-processing is to zero the signal since the raw signal is based on an origin located at the top left corner of the image. The zero-ed signal is produced by subtracting the median of the signal from each point in the signal. The second step of post-processing is to scale the signal. The scaling factor (amplitude resolution V), shown in equation 4, is the product of: the inverse of the grid size, which converts the signal from units of pixels to millimeters (mm); the inverse of the user-supplied voltage scale, which converts units of millimeters (mm) to millivolts (mV); and 1000 to convert from mV to microvolts (μV).

$$V_{ECG} = \frac{1}{V_{image}} \times \frac{1}{V_{scale}} \times 1000 \quad \text{(eq 4),}$$

where V_{ECG} is amplitude resolution in μV/pixel; V_{image} is image resolution in pixels/mm; V_{scale} is printed ECG voltage scale in mm/mV (usually 10 mm = 1 mV).

The extracted signals are padded with zeros at the left and right sides, such that every signal has the same length. First, the user-supplied start times are used to pad signals on the left side. The number of pixels to pad is determined by dividing the start time (in seconds) by the horizontal scaling factor (sampling rate *F)*, defined in equation 5.

$$F = \frac{1}{F_{image}} \times \frac{1}{F_{scale}} \quad \text{(eq 5)},$$

where F is sampling rate in seconds per pixel; F_{image} is image sampling rate resolution in pixels/mm; F_{scale} is printed ECG sampling rate scale in mm/second (usually 25 mm = 1 second).

If the start time is 0 seconds, no padding is applied. The signals, which have been padded on the left if needed, are padded with zeroes on the right to reach the length of the longest signal. No right padding is applied to the longest signal. After integration, the signal data is passed back to the GUI for the user to preview (Supplemental Figure 2B) and save to a file. Users can choose to save the file in plain text (.txt) or comma-separated value (.csv) formats. We did not smooth or otherwise altered the extracted ECG signal.

2.3. Validation of the automated digitizing algorithm

For validation, we assessed the agreement in the standard ECG and VCG GEH measurements, performed on three types of ECG signal: (1) digitally recorded, simultaneous ECG leads, (2) digitally recorded, asynchronous ECG leads, and (3) digitized, asynchronous ECG leads. Validation of clinical ECG diagnosis was conducted by two investigators (HP, LGT) by comparing clinical ECG diagnosis (heart rhythm, left or right bundle branch block, intraventricular conduction delay, left or right ventricular hypertrophy) on listed above 3 types of ECG signal.

2.3.1. ECG and VCG measurements on digitally recorded, simultaneous ECG leads—

Using a 10-second simultaneously recorded 12-lead digital ECG signal, we detected the origin of the heart vector and comprised the time-coherent global XYZ median beat as previously described.[25] Using previously validated algorithms,[26, 27] we detected ECG fiducial points on the median beat vector magnitude signal. The accuracy of automated fiducial point detection was confirmed by two investigators (KTH, HP) using visual aid. Next, we measured traditional ECG metrics (PR, QRS, QT, and Bazett-corrected QTc intervals). We used reported by the GE 12SL algorithm measurements on a 10-second simultaneously digitally recorded 12-lead ECG signal. In addition, VCG GEH metrics (area-based and peak-based spatial ventricular gradient [SVG] magnitude, azimuth, and elevation, spatial QRS-T angle, sum absolute QRST integral [SAIQRST], and vector magnitude (VM) QT integral [VMQTi]), as well as separate VM QRS and VM T areas were measured as previously described.[25, 28]

2.3.2. ECG and VCG measurements on digitized asynchronous ECG leads—

On the digitized ECG signal, we selected one complete (artifact-free PQRST waveform) representative cardiac beat on each out of eight leads: I, II, V1-V6. We used a median filter with a moving window of length 1/10th of sampling frequency to remove baseline

wander.[29] Furthermore, high frequency (> 150 Hz) noise and artifacts were removed using synchrosqueezing transform with morlet wavelet as previously described.[30] Next, the time point of the maximum absolute |dV/dt| QRS value was automatically detected on each selected cardiac beat. All eight cardiac beats were aligned using the detected maximum absolute |dV/dt| time point and converted to XYZ using Kors transformation matrix,[31] which led to the construction of a representative global XYZ beat. Then, the origin of the heart vector was identified.[25] As described above, we used previously validated algorithms[26, 27] to detect ECG fiducial points. The accuracy of automated fiducial point detection was confirmed (and corrected if needed) by two investigators (KTH, HP) using visual aid.

2.3.4. ECG and VCG measurements on digitally recorded asynchronous ECG leads.—To validate the digitization process and to distinguish an error introduced by an asynchronous cardiac beat from the digitization error, we constructed the representative global XYZ beat using the digitally recorded asynchronous ECG signal. We selected the same cardiac beats on the same ECG leads that were used for the analysis of digitized ECG signals. Then, all the signal processing steps were performed as described above.

2.3.5. Assessment of the agreement—To compare ground truth (digitally recorded) and digitized signals, we downsampled digitized signal to 500 Hz and then calculated mean sample-by-sample difference, and root mean square error (RMSE), and correlation for VM PQRST complex. The agreement between ECG and VCG measurements on the digitally recorded time-coherent median beat, representative asynchronous digitized beat, and the representative asynchronous digitally recorded beat was assessed by Bland-Altman analysis.[32, 33] We calculated the degree of the agreement as to the bias (the absolute mean difference) with 95% limits of agreement (LOA). The Bradley-Blackwood procedure was used to compare the means and variances of the 2 compared measurements simultaneously. Bonferroni-adjusted significance of the Bradley-Blackwood F-test ($P<0.001$) indicated a statistically significant correlation of compared means and variances, implying biased estimates of the Bland-Altman analysis. Precision was defined as 100% minus relative % bias. Interclass correlation coefficient (ICC), equivalent to Cronbach's alpha statistic,[34] was calculated for standardized variables (in the scale to mean 0 and variance 1). Lin's concordance correlation coefficient ρ_c was calculated to describe the strength of agreement: >0.99 indicated almost perfect agreement; 0.95–0.99, substantial agreement; 0.90–0.95, moderate agreement; <0.90, poor agreement. As the SVG azimuth variables are circular (ranging from −180° to +180°), to calculate relative bias and ICC, SVG azimuth variables were transformed by doubling their value and adding 360. The agreement assessment was performed using STATA MP 17.0 (StataCorp LLC, College Station, TX, USA).

Results

1.3. Study population

The study population included 230 subjects. The study dataset was randomly divided into development (n=150; 65%) and validation (n=80; 35%) subsets. There were no statistically significant differences in clinical and demographic characteristics of subjects included in

development and validation datasets (Table 2). Approximately one-quarter of subjects were female, and more than 80% were white. About half of the participants were healthy, and their ECGs were normal, whereas another half had a history of cardiovascular disease and abnormal ECG.

3.2. Validation results

Examples of digitized 12-lead ECG and VCG are shown in Supplemental Figures 3 and 4. There was full 100% agreement in clinical ECG diagnosis made using digitized versus digitally recorded ECG signal. There was also 100% agreement between two investigators, and between investigators and clinical ECG diagnosis listed in a medical record. For the quantitative assessment of the agreement, we excluded the ECGs (n=40; 50%) with obvious visible errors of the digitization, assessed by two investigators (KTH, HP), because the goal of this study was to assess the performance of this algorithm, whereas ECG images that failed digitization had to undergo manual fine-tuning of the digitization process. [3] Examples of digitization errors are shown in Supplemental Figure 5. The total time processing for a one ECG lead was 3-5 seconds.

3.2.1. The sample-by-sample difference, RMSE, and correlation between ground truth and digitized signals—The sample-per-sample comparison of digitally recorded and digitized signals showed a very high correlation (0.977), a small mean difference (9.3 μV), and RMSE (25.9 μV). The error was largely consistent across ECG leads (Table 3).

3.2.2. Agreement between digitally recorded and digitized asynchronous representative beat—The precision of traditional ECG measurements (PR, QRS, QT intervals) assessed on digitized versus digitally recorded cardiac beat was substantial or nearly perfect, ranging from 97.2% to 99.1% (Table 4). Accordingly, the mean bias was small (up to 4 ms). However, their agreement measured by ρ_c was poor, and ICC was < 0.9, consistently with wide LOA (Table 4 and Figures 7–10).

The precision and agreement of area-based GEH VCG measurements were better than traditional ECG measurements, with ICC > 0.9 and ρ_c up to 0.97, thus indicating substantial agreement. Mean bias and 95%LOA were within a clinically acceptable range for area-based GEH metrics (Figures 11–12). QRS area and T area also demonstrated nearly perfect agreement, with Lin's concordance of 0.99 and ICC of 0.997, the precision of 99%, and the mean bias of 0.25 mVms. The precision and agreement of peak-based GEH VCG measurement were variable, with some coefficients below 0.9 (or less than 90%), whereas other (e.g., peak SVG azimuth and elevation) demonstrated nearly perfect (~98%) agreement. Notably, less-than-perfect precision and agreement of peak-based VCG metrics were comparable to that of traditional ECG metrics (QRS duration, QT interval).

3.2.3. Agreement between digitally recorded asynchronous beat and time-coherent median beat—There was a substantial difference in agreement observed for area-based versus peak-based GEH VCG measurements. All but one area-based GEH VCG measurements showed substantial agreement, reflected by ICC and ρ_c >0.95 and

high precision ≥ 95%. The mean bias for area-based VCG angles was minor (~1°), with clinically acceptable 95%LOA (±20-30°). However, the mean bias for peak-based VCG angles was substantial (~ 10°), and 95% LOA was clinically unacceptable (± 60-90°). One exception was SVG elevation, demonstrating higher precision and agreement if measured by peak-based (rather than area-based) metrics. (Table 4). Precision and agreement for traditional ECG measurements ranged from poor to moderate.

3.2.4. Agreement between digitized asynchronous representative beat and digitally recorded time-coherent median beat—

Out of all ECG and VCG measurements (Table 4), SAIQRST, VMQTi, and area-based SVG magnitude showed the highest agreement, precision, and concordance, the slightest mean bias (2-3 mV*ms), and clinically acceptable 95%LOA ±20-30 mV*ms (Figures 11–12). Precision and agreement for other area-based GEH VCG measurements were also acceptable, ranging from moderate to substantial, with clinically acceptable bias. However, the agreement and precision for some (but not all) peak-based GEH VCG metrics were lesser than for area-based VCG metrics. A precision, agreement, and concordance observed for traditional ECG metrics were similar to those reported for pairs of digitally recorded asynchronous beat and time-coherent median beat.

Discussion

In this work, we developed and validated a new algorithm for paper-ECG digitization, converting a scan (i.e., image) of a printed on paper ECG into a digital ECG signal. We implemented a novel dynamic programming approach that preserved the high resolution of the ECG signal. For the first time, we provided an open-source Python code that facilitates further development and implementation of the developed ECG digitization tool. Furthermore, we compared the sources of disagreement between the ECG and VCG measurements that were performed on a digitally recorded and digitized ECG signal. We identified the heart rate (cardiac cycle length) and morphological differences between a median beat that was constructed using eight digitally, simultaneously recorded ECG leads versus a representative beat constructed using asynchronous ECG leads as the major source of the disagreement. Notably, in a successfully digitized ECG signal, SAIQRST, VMQTi, and other area-based GEH VCG metrics showed substantial, clinically acceptable agreement. In contrast, peak-based VCG metrics as well as PR, QRS, and QT intervals demonstrated moderate to poor agreement. As reported in the present study, bias with 95%LOA should be considered by future investigators planning analyses of digitized ECG.

4.1. Comparison of the paper-ECG digitization methods

Several other algorithms for paper ECG digitization have been previously developed.[3, 7, 10] Additional references are provided in the Supplement. Unlike several earlier digitizing applications that scaled-down image resolution to reduce the computational cost,[3, 35] we elected to use high-resolution images (600 dpi) to output a high-resolution ECG signal, taking advantage of computationally-efficient Python libraries.[21] Furthermore, we preserved the high resolution of the digitized ECG signal, providing users an opportunity to implement their preferred subsequent ECG signal processing approach. Importantly,

our algorithm did not “remove the grid from the ECG signal,” but instead, utilized a different approach – simultaneous extraction of both types of signals – the grid and the ECG waveform. Therefore, we did not encounter the removal of the ECG signal features observed by previous investigators.[35, 36] Several recent algorithms incorporated somewhat similar approaches.[37, 38] In comparison to other algorithms, we utilized the strengths of the *Viterbi* dynamic programming, which directly computes the global best path as defined by the score function. In contrast, the typical optimization technique used by active contour implementation is gradient descent, which finds local minima but is not guaranteed to find the global minimum. However, the run-time of the *Viterbi*-based algorithm depends upon the number of possible signal pixels under consideration, which means a longer processing time for noisy images that can be perceived as a disadvantage. Conversely, the runtime of active contour algorithms may be constant if the implementation runs a constant number of iterations of gradient descent. There are also similarities between algorithms. The *Viterbi*-based algorithm has parameters that permit constraining the length and the rigidity of the generated contour similarly to the effects of the active contour parameters [*alpha*] and [*beta*], respectively. Both algorithms are challenging to parallelize due to many interdependencies between the steps. In the *Viterbi*-based algorithm, there is a dependency between the score of one column and the computed score for the next column, whereas in the active contour algorithm, there is a dependency between each step in time. This can be addressed in both cases by synchronization locks that force the steps to occur in order without any overlap.

Nonetheless, we acknowledge the shortcomings of the presented tool. Only half of the ECGs in the validation dataset were amenable for a fully automated digitization, whereas the second half might require manual fine-tuning of the digitization, if desired by investigators. To provide the path forward to facilitate further development of paper-ECG digitizing tools, we provided our developed software code on GitHub, a convenient environment for software developers. Notably, all digitized ECGs allowed accurate clinical ECG interpretation.

We acknowledge that the signal extraction algorithm does not perform well at sharp turning points (e.g., near the peaks of the QRS complex), which has been a common problem in ECG digitization.[3, 7] In the future, this may be addressed by (1) using active contours with a dynamic low-pass filter for signal extraction or (2) adding a post-processing step that identifies turning points and pulls the estimated signal to the pixels at the outer edge of the turning point. Furthermore, there may be errors in the signal extraction algorithm at the left and right edges. This may be addressed by (1) running *Viterbi* forward and backward, (2) using active contours for signal extraction, or (3) implementing a more intelligent approach to find the best path.

4.2. Simultaneously recorded versus asynchronous ECG leads

As expected, we observed significant differences in the VCG morphology between a median beat comprised of 10-second digitally recorded simultaneous ECG leads, and a representative cardiac beat, constructed of digitally recorded, asynchronous ECG leads. Differences in the VCG morphology translated into differences in the ECG and VCG measurements, which must be considered when comparing the results of different studies. Importantly, we observed clinically meaningful bias in heart rate and QT interval

measurements (~ 20 ms). Similarly, Holkeri et al.[10] compared the QT interval measured on asynchronous ECG leads and observed clinically important differences (>20 ms) in nearly 25% of their study population. Furthermore, Hingorani et al.[13] described additional contributions of the printer that affected the noted differences in the ECG measurements.

In the present study, we conducted the most comprehensive quantitative assessment of agreement between the ECG and VCG measurements, performed on three different types of cardiac beats: (1) a time-coherent median beat constructed using 10-second digitally recorded, simultaneous ECG leads, (2) a representative asynchronous beat constructed using digitally recorded, asynchronous ECG leads, and (3) a representative asynchronous beat constructed using digitized, asynchronous ECG leads. We reported a mean bias with 95% LOA, precision, ICC, and concordance coefficients. As reported in this study, the differences between the types of ECG signals must be considered for planning future studies and interpreting previously conducted analyses. While further improvement in the digitization algorithms can reduce an error of the digitization procedure itself, fundamental differences between simultaneously recorded and asynchronous ECG leads remain. Area-based GEH VCG metrics appear to be robust and insensitive to different types of ECG signals and can be recommended for measurement on digitized ECGs. Asynchronous ECG lead recording affects peak-based VCG metrics to a greater degree compared to the area-based VCG metrics. The major reason for that is the effect of respiration on the ECG signal amplitude, which is utilized in algorithms extracting a respiration signal from the surface ECG.[39]. Our recent large study (> 4000 participants) consistently showed that the reproducibility of peak-based VCG metrics was slightly inferior to that of area-based VCG metrics.[40]

Our study has important clinical implications. First, we provided the source code in Python so that the research community can work by completing it and improving it. Having open-source code opens opportunity for analysis of ECG images by multiple clinical investigators who have the data for analysis, but don’t have funding. Second, we provided a comprehensive review of the state of the art and offered a thorough, rigorous methodology of validation. Third, we presented clinically acceptable agreement when comparing parameters such as SAIQRST, VMQTi, and other area based GEH VCG metrics between the digitized ECG signals and those ECG digitally recorded, which supports their implementation in clinical practice.

4.3. Limitations

Several limitations of the study must be considered. First, while we attempted to comprise the diverse developmental dataset, including normal ECGs of healthy individuals, abnormal ECGs of patients with cardiovascular diseases, and printed on paper ECGs with a variable degree of quality, there is a chance that our development dataset did not include all possible types of ECG images. All of the thresholds were heuristic and have been selected by testing a range of values in the developmental dataset to ensure the best performance for all ECG images. Therefore, different thresholds of the algorithm’s decisions might improve its performance on different types of paper-ECG images. Future studies are needed to address this limitation. Notably, we provided open-source software code that will help to continue further improvement of the ECG digitizing tool by future investigators. Only normal sinus

rhythm ECGs were included in this study, similarly to other ECG digitizing studies.[3, 13] Further studies are needed to assess the performance of the ECG digitizing algorithms in cardiac arrhythmias, and in different patient populations. Finally, we did not investigate the effect of degradation of the input image quality and the poor scanning quality on the output of our algorithm, which should be investigated in future studies.

Conclusions

The newly developed and validated algorithm for paper-ECG digitization converted an image printed on a paper ECG into a digital ECG signal with high precision. The differences in the cardiac cycle length and the VCG morphology between a time-coherent median beat, comprised of 10-second simultaneously recorded ECG leads and a single cardiac beat, comprised of asynchronous ECG leads, contributed the most to the disagreement between ECG measurements on digitally recorded and digitized ECGs. Area-based GEH VCG metrics preserved the clinically acceptable agreement, thus, can be recommended for measurement on the digitized ECG. Future work is needed in improvement of the digitization at the sharp turning points, for the missing portions of ECG signal, and for noisy ECG images.

Supplementary Material

Refer to Web version on PubMed Central for supplementary material.

Funding and Acknowledgment:

This work was partially supported by the National Institutes of Health (HL118277), Medical Research Foundation of Oregon, and OHSU President Bridge funding to Tereshchenko.

2. References

Several other algorithms for paper ECG digitization have been previously developed. Full references list is provided below.[3, 7, 10, 35–38, 41–44]

[1]. Kligfield P, Badilini F, Brown B, Helfenbein E, Kohls M, The ISCE ECG genome pilot challenge: A 2004 progress report, Journal of Electrocardiology, 37 (2004) 144–148. [PubMed: 15534824]

[2]. Stockbridge N, Points to consider in electrocardiogram waveform extraction, Journal of Electrocardiology, 38 (2005) 319–320. [PubMed: 16216603]

[3]. Badilini F, Erdem T, Zareba W, Moss AJ, ECGScan: a method for conversion of paper electrocardiographic printouts to digital electrocardiographic files, J Electrocardiol, 38 (2005) 310–318. [PubMed: 16216602]

[4]. Tereshchenko LG, Sotoodehnia N, Sitlani CM, Ashar FN, Kabir M, Biggs ML, Morley MP, Waks JW, Soliman EZ, Buxton AE, Biering-Sorensen T, Solomon SD, Post WS, Cappola TP, Siscovick DS, Arking DE, Genome-Wide Associations of Global Electrical Heterogeneity ECG Phenotype: The ARIC (Atherosclerosis Risk in Communities) Study and CHS (Cardiovascular Health Study), J Am Heart Assoc, 7 (2018) e008160. [PubMed: 29622589]

[5]. Pollard JD, Haq KT, Lutz KJ, Rogovoy NM, Paternostro KA, Soliman EZ, Maher J, Lima JAC, Musani SK, Tereshchenko LG, Electrocardiogram machine learning for detection of cardiovascular disease in African Americans: the Jackson Heart Study, Eur Heart J Digit Health, 2 (2021) 137–151. [PubMed: 34048510]

[6]. Waks JW, Sitlani CM, Soliman EZ, Kabir M, Ghafoori E, Biggs ML, Henrikson CA, Sotoodehnia N, Biering-Sorensen T, Agarwal SK, Siscovick DS, Post WS, Solomon SD,

Buxton AE, Josephson ME, Tereshchenko LG, Global Electric Heterogeneity Risk Score for Prediction of Sudden Cardiac Death in the General Population: The Atherosclerosis Risk in Communities (ARIC) and Cardiovascular Health (CHS) Studies, Circulation, 133 (2016) 2222–2234. [PubMed: 27081116]

[7]. Waits GS, Soliman EZ, Digitizing paper electrocardiograms: Status and challenges, J Electrocardiol, 50 (2017) 123–130. [PubMed: 27658690]

[8]. Norman JE, Bailey JJ, Berson AS, Haisty WK, Levy D, Macfarlane PM, Rautaharju PM, NHLBI workshop on the utilization of ECG databases: Preservation and use of existing ECG databases and development of future resources, Journal of Electrocardiology, 31 (1998) 83–89. [PubMed: 9588653]

[9]. Brisk R, Bond R, Banks E, Piadlo A, Finlay D, McLaughlin J, McEneaney D, Deep learning to automatically interpret images of the electrocardiogram: Do we need the raw samples?, Journal of Electrocardiology, 57 (2019) S65–S69.

[10]. Holkeri A, Eranti A, Kenttä TV, Noponen K, Haukilahti MAE, Seppänen T, Junttila MJ, Kerola T, Rissanen H, Heliövaara M, Knekt P, Aro AL, Huikuri HV, Experiences in digitizing and digitally measuring a paper-based ECG archive, Journal of Electrocardiology, 51 (2018) 74–81. [PubMed: 29031413]

[11]. Tereshchenko LG, Cheng A, Park J, Wold N, Meyer TE, Gold MR, Mittal S, Singh J, Stein KM, Ellenbogen KA, SMART-AV Trial Investigators, Novel measure of electrical dyssynchrony predicts response in cardiac resynchronization therapy: Results from the SMART-AV Trial, Heart Rhythm, 12 (2015) 2402–2410. [PubMed: 26272523]

[12]. Kligfield P, Overview of the ISCE ECG “genome project”, Journal of Electrocardiology, 36 (2003) 163–165. [PubMed: 14716619]

[13]. Hingorani P, Karnad DR, Panicker GK, Deshmukh S, Kothari S, Narula D, Differences between QT and RR intervals in digital and digitized paper electrocardiograms: contribution of the printer, scanner, and digitization process, Journal of Electrocardiology, 41 (2008) 370–375. [PubMed: 18482732]

[14]. Kligfield P, Gettes LS, Bailey JJ, Childers R, Deal BJ, Hancock EW, van HG, Kors JA, Macfarlane P, Mirvis DM, Pahlm O, Rautaharju P, Wagner GS, Josephson M, Mason JW, Okin P, Surawicz B, Wellens H, Recommendations for the standardization and interpretation of the electrocardiogram: part I: the electrocardiogram and its technology a scientific statement from the American Heart Association Electrocardiography and Arrhythmias Committee, Council on Clinical Cardiology; the American College of Cardiology Foundation; and the Heart Rhythm Society endorsed by the International Society for Computerized Electrocardiology, J Am Coll.Cardiol, 49 (2007) 1109–1127. [PubMed: 17349896]

[15]. Kabir MM, Perez-Alday EA, Thomas J, Sedaghat G, Tereshchenko LG, Optimal configuration of adhesive ECG patches suitable for long-term monitoring of a vectorcardiogram, J Electrocardiol, 50 (2017) 342–348. [PubMed: 28069275]

[16]. Thomas JA, Perez-Alday EA, Hamilton C, Kabir MM, Park EA, Tereshchenko LG, The utility of routine clinical 12-lead ECG in assessing eligibility for subcutaneous implantable cardioverter defibrillator, Comput Biol Med, 102 (2018) 242–250. [PubMed: 29754992]

[17]. Thomas JA, A.P. AE, Junell A, Newton K, Hamilton C, Li-Pershing Y, German D, Bender A, Tereshchenko LG, Vectorcardiogram in athletes: The Sun Valley Ski Study, Ann Noninvasive Electrocardiol, 24 (2019) e12614. [PubMed: 30403442]

[18]. Wang L, Javadekar N, Rajagopalan A, Rogovoy NM, Haq KT, Broberg CS, Tereshchenko LG, Eligibility for subcutaneous implantable cardioverter-defibrillator in congenital heart disease, Heart Rhythm, 17 (2020) 860–869. [PubMed: 32354451]

[19]. Python: cv2.adaptiveThreshold. https://docs.opencv.org/2.4/modules/imgproc/doc/miscellaneous_transformations.html. Accessed 05.17.2021.

[20]. Sedgewick R, Wayne KD, Algorithms, 4th ed., Addison-Wesley, Upper Saddle River, NJ, 2011.

[21]. Virtanen P, Gommers R, Oliphant TE, Haberland M, Reddy T, Cournapeau D, Burovski E, Peterson P, Weckesser W, Bright J, van der Walt SJ, Brett M, Wilson J, Millman KJ, Mayorov N, Nelson ARJ, Jones E, Kern R, Larson E, Carey CJ, Polat I, Feng Y, Moore EW, VanderPlas J, Laxalde D, Perktold J, Cimrman R, Henriksen I, Quintero EA, Harris CR, Archibald AM,

Ribeiro AH, Pedregosa F, van Mulbregt P, SciPy C, SciPy 1.0: fundamental algorithms for scientific computing in Python, Nature methods, 17 (2020) 261–272. [PubMed: 32015543]

[22]. Otsu N, A Threshold Selection Method from Gray-Level Histograms, IEEE Transactions on Systems, Man, and Cybernetics, 9 (1979) 62–66.

[23]. Huang L, Advanced Dynamic Programming in Semiring and Hypergraph Frameworks, Coling 2008 Organizing Committee, Manchester, UK, 2008, pp. 1–18.

[24]. Granger CWJ, Prediction with a Generalized Cost of Error Function, Journal of the Operational Research Society, 20 (1969) 199–207.

[25]. Perez-Alday EA, Li-Pershing Y, Bender A, Hamilton C, Thomas JA, Johnson K, Lee TL, Gonzales R, Li A, Newton K, Tereshchenko LG, Importance of the heart vector origin point definition for an ECG analysis: The Atherosclerosis Risk in Communities (ARIC) study, Comput Biol Med, 104 (2019) 127–138. [PubMed: 30472495]

[26]. Pan J, Tompkins W, A real-time QRS detection algorithm, IEEE transactions on bio-medical engineering, 32 (1985) 230–236. [PubMed: 3997178]

[27]. Zhou SH, Helfenbein ED, Lindauer JM, Gregg RE, Feild DQ, Philips QT interval measurement algorithms for diagnostic, ambulatory, and patient monitoring ECG applications, Ann Noninvasive Electrocardiol, 14 Suppl 1 (2009) S3–8. [PubMed: 19143739]

[28]. Perez-Alday EA, Bender A, German D, Mukundan SV, Hamilton C, Thomas JA, Li-Pershing Y, Tereshchenko LG, Dynamic predictive accuracy of electrocardiographic biomarkers of sudden cardiac death within a survival framework: the Atherosclerosis Risk in Communities (ARIC) study, BMC cardiovascular disorders, 19 (2019) 255. [PubMed: 31726979]

[29]. de Chazal P, Heneghan C, Sheridan E, Reilly R, Nolan P, O'Malley M, Automated processing of the single-lead electrocardiogram for the detection of obstructive sleep apnoea, IEEE transactions on bio-medical engineering, 50 (2003) 686–696. [PubMed: 12814235]

[30]. Kabir MM, Tereshchenko LG, Development of Analytical Approach for an Automated Analysis of Continuous Long-Term Single Lead ECG for Diagnosis of Paroxysmal Atrioventricular Block, Computing in cardiology, 41 (2014) 913–916. [PubMed: 25541629]

[31]. Kors JA, van HG, Sittig AC, van Bemmel JH, Reconstruction of the Frank vectorcardiogram from standard electrocardiographic leads: diagnostic comparison of different methods, Eur.Heart J, 11 (1990) 1083–1092. [PubMed: 2292255]

[32]. Bland JM, Altman DG, Statistical methods for assessing agreement between two methods of clinical measurement, Lancet, 1 (1986) 307–310. [PubMed: 2868172]

[33]. Huang T, James CA, Tichnell C, Murray B, Xue J, Calkins H, Tereshchenko LG, Statistical evaluation of reproducibility of automated ECG measurements: an example from arrhythmogenic right ventricular dysplasia/cardiomyopathy clinic, Biomedical signal processing and control, 13 (2014) 23–30. [PubMed: 24883077]

[34]. Bravo G, Potvin L, Estimating the reliability of continuous measures with Cronbach's alpha or the intraclass correlation coefficient: toward the integration of two traditions, Journal of clinical epidemiology, 44 (1991) 381–390. [PubMed: 2010781]

[35]. Ravichandran L, Harless C, Shah AJ, Wick CA, Mcclellan JH, Tridandapani S, Novel tool for complete digitization of paper electrocardiography data, IEEE journal of translational engineering in health and medicine, 1 (2013) 1800107–1800107. [PubMed: 26594601]

[36]. Swamy P, Jayaraman S, Chandra MG, An improved method for digital time series signal generation from scanned ECG records, 2010 International Conference on Bioinformatics and Biomedical Technology, 2010, pp. 400–403.

[37]. Baydoun M, Safatly L, Hassan OKA, Ghaziri H, Hajj AE, Isma'eel H, High Precision Digitization of Paper-Based ECG Records: A Step Toward Machine Learning, IEEE Journal of Translational Engineering in Health and Medicine, 7 (2019) 1–8.

[38]. Li Y, Qu Q, Wang M, Yu L, Wang J, Shen L, He K, Deep learning for digitizing highly noisy paper-based ECG records, Computers in Biology and Medicine, 127 (2020) 104077. [PubMed: 33171291]

[39]. Helfenbein E, Firoozabadi R, Chien S, Carlson E, Babaeizadeh S, Development of three methods for extracting respiration from the surface ECG: A review, Journal of Electrocardiology, 47 (2014) 819–825. [PubMed: 25194875]

[40]. Haq KT, Lutz KJ, Peters KK, Craig NE, Mitchell E, Desai AK, Stencel NWL, Soliman EZ, Lima JAC, Tereshchenko LG, Reproducibility of global electrical heterogeneity measurements on 12-lead ECG: The Multi-Ethnic Study of Atherosclerosis, J Electrocardiol, 69 (2021) 96–104. [PubMed: 34626835]

[41]. Sbrollini A, Agostinelli A, Marcantoni I, Morettini M, Burattini L, Di Nardo F, Fioretti S, Burattini L, eCTG: an automatic procedure to extract digital cardiotocographic signals from digital images, Computer methods and programs in biomedicine, 156 (2018) 133–139. [PubMed: 29428065]

[42]. Wang S, Zhang S, Li Z, Huang L, Wei Z, Automatic digital ECG signal extraction and normal QRS recognition from real scene ECG images, Computer methods and programs in biomedicine, 187 (2020) 105254. [PubMed: 31830698]

[43]. Kao T, Len-Jon H, Yui-Han L, Tzong-Huei L, Chia-Hung H, Computer analysis of the electrocardiograms from ECG paper recordings, 2001 Conference Proceedings of the 23rd Annual International Conference of the IEEE Engineering in Medicine and Biology Society, 2001, pp. 3232–3234 vol.3234.

[44]. Wang JT, Mital DP, A microcomputer-based prototype for ECG paper record conversion, Journal of Network and Computer Applications, 19 (1996) 295–307.

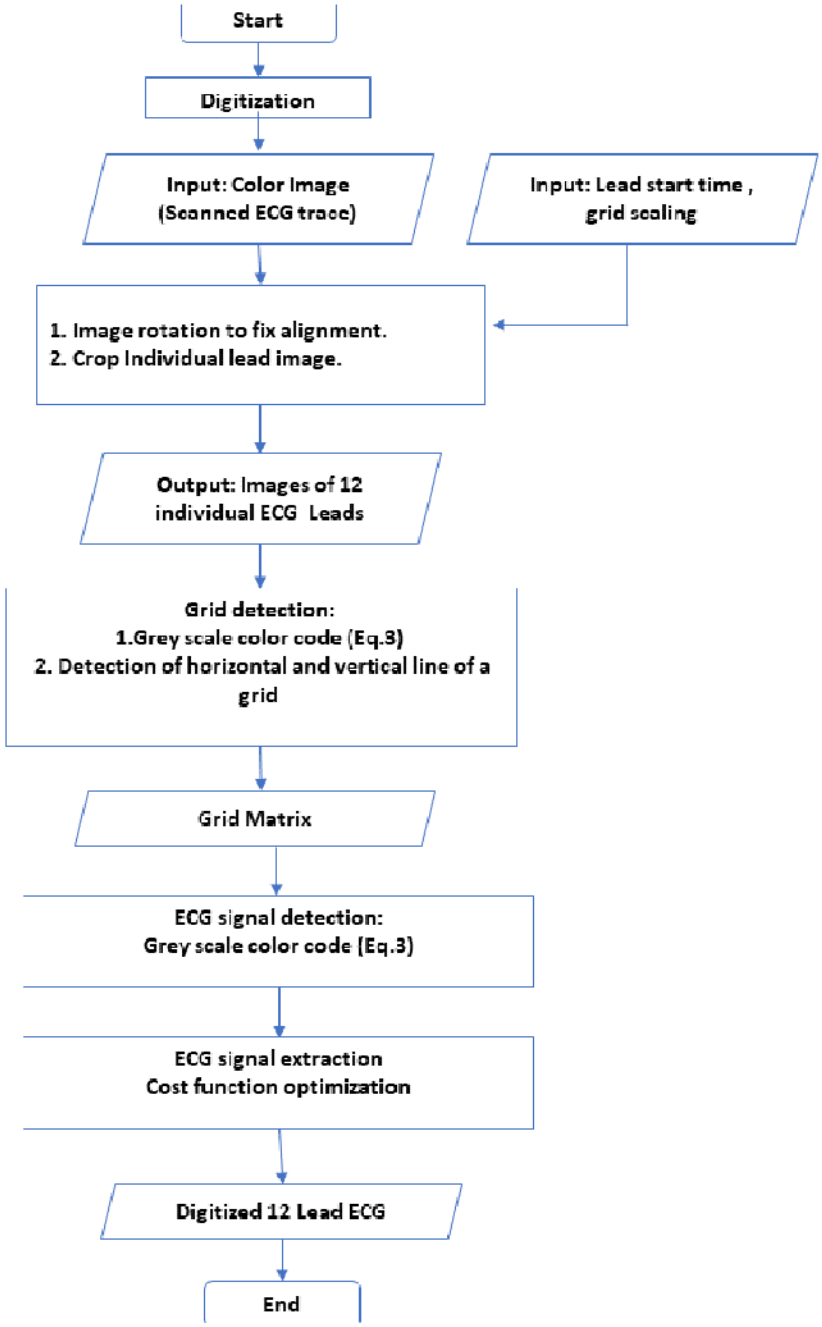

Figure 1.
Flowchart of the developed algorithm.

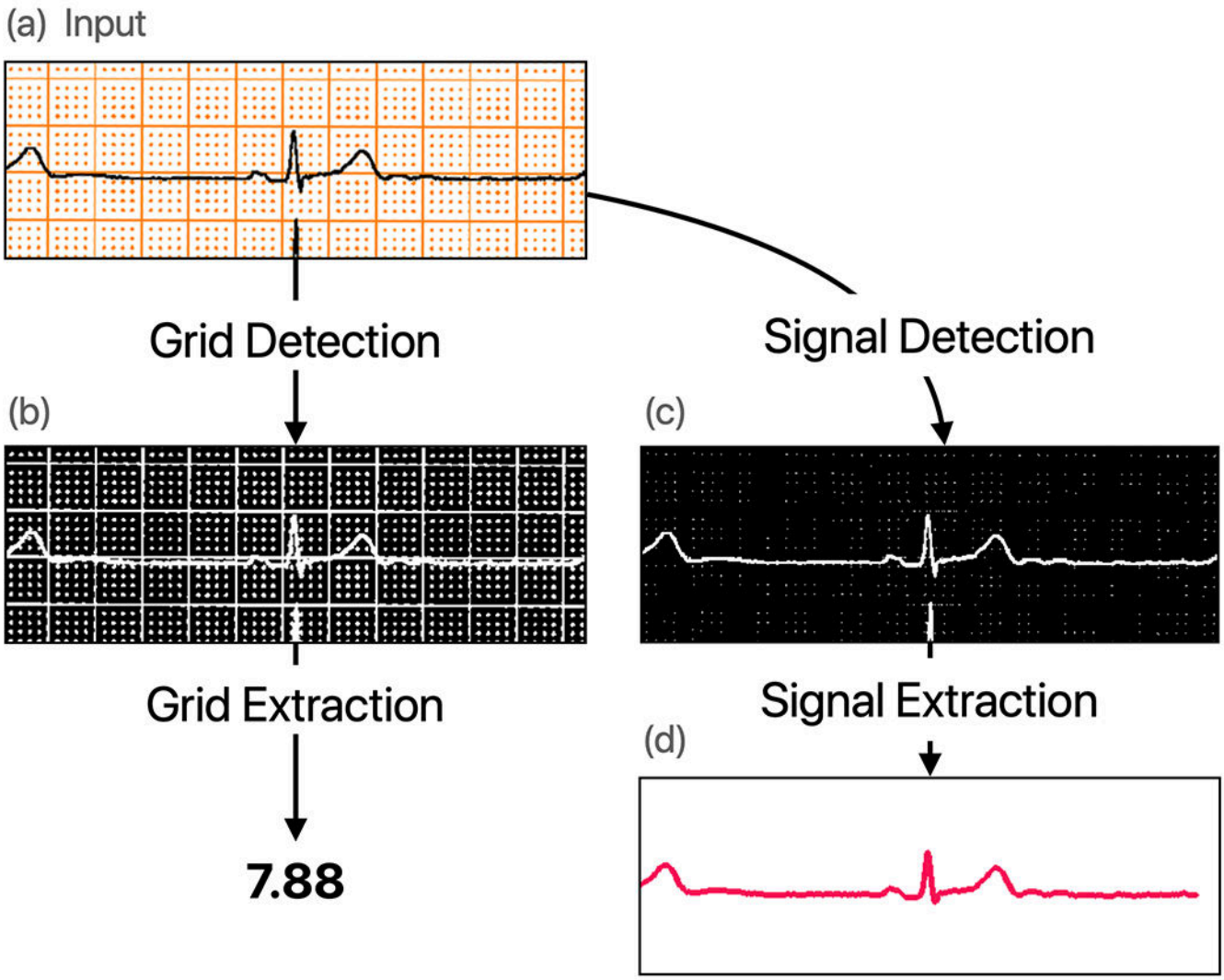

Figure 2.
The overview and the representative example of the digitization process.

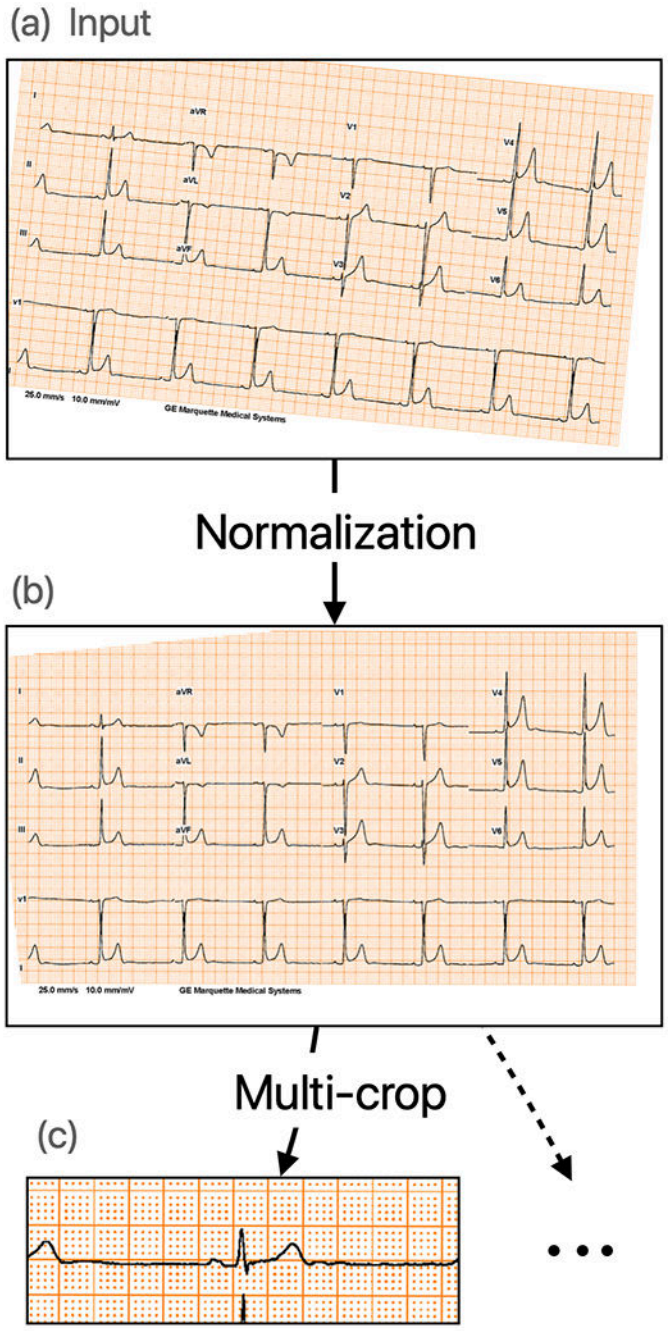

Figure 3.

Preparation of the ECG mage for digitizing. The input image is rotated by 5.5 degrees (specified by user or autorotation) to produce the normalized image. Then, the normalized image is cropped to x=73, y=237, width=488, and height=165 to produce the cropped lead image. The application may produce up to 12 cropped lead images, but only one is shown for brevity.

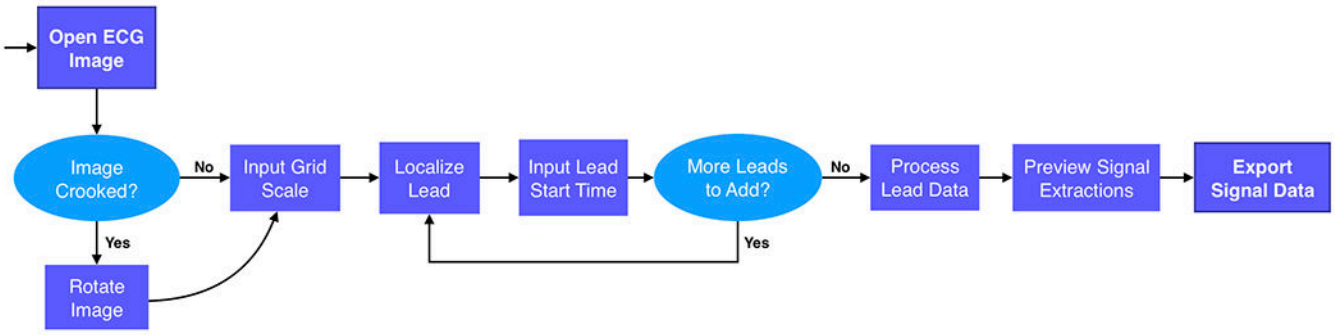

Figure 4.
The typical user workflow when using the application.

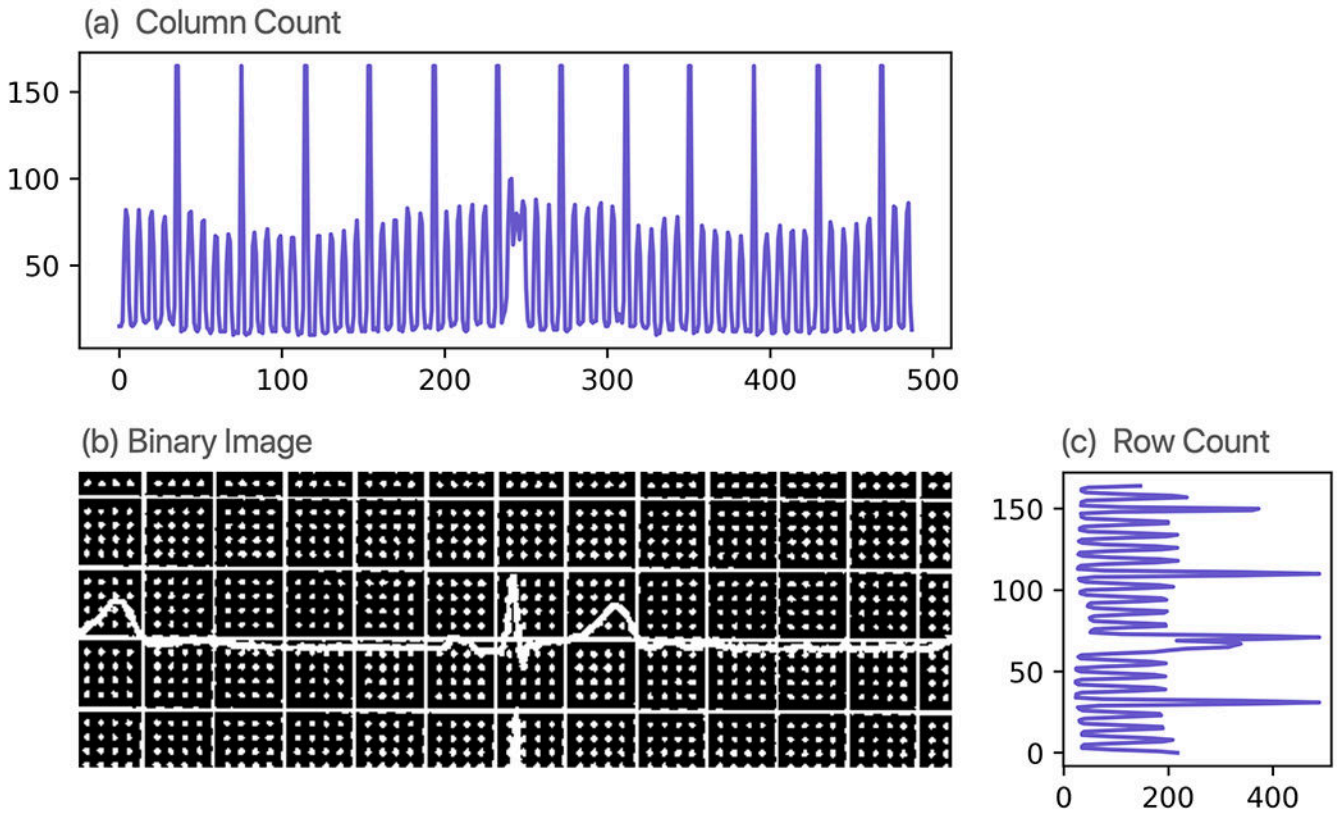

Figure 5.

Grid extraction. The column count (a) and the row count (c) for the binary image input (b) are shown. The count signals have a comb-like shape where teeth occur at grid line locations. In this example, the grid involves some dotted lines, which results in lower counts for those rows or columns, but the results of frequency analysis are not different from a grid with all solid lines.

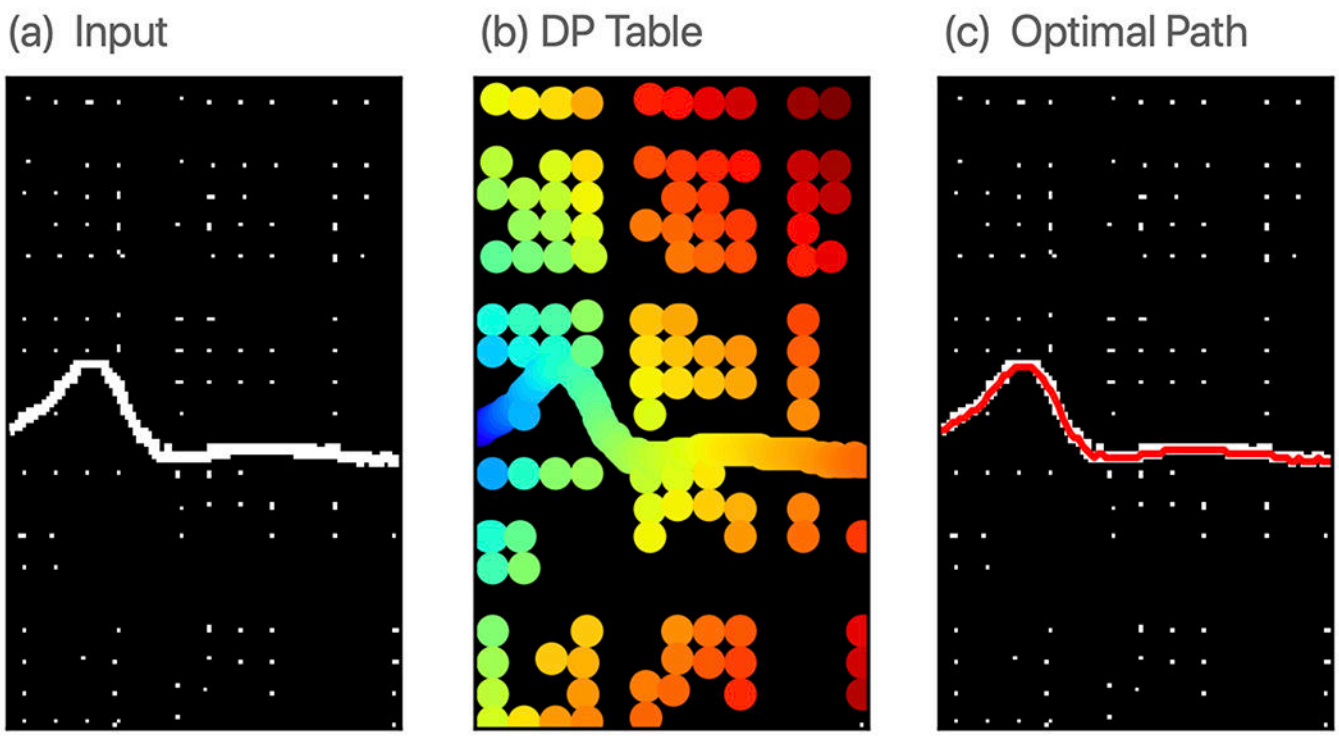

Figure 6.
An example of the Viterbi dynamic programming table. The input image (a) is processed by the Viterbi dynamic programming algorithm. The total cost for the path to each point is based on the dynamic programming table (b). The minimal total cost is selected as the best path (c).

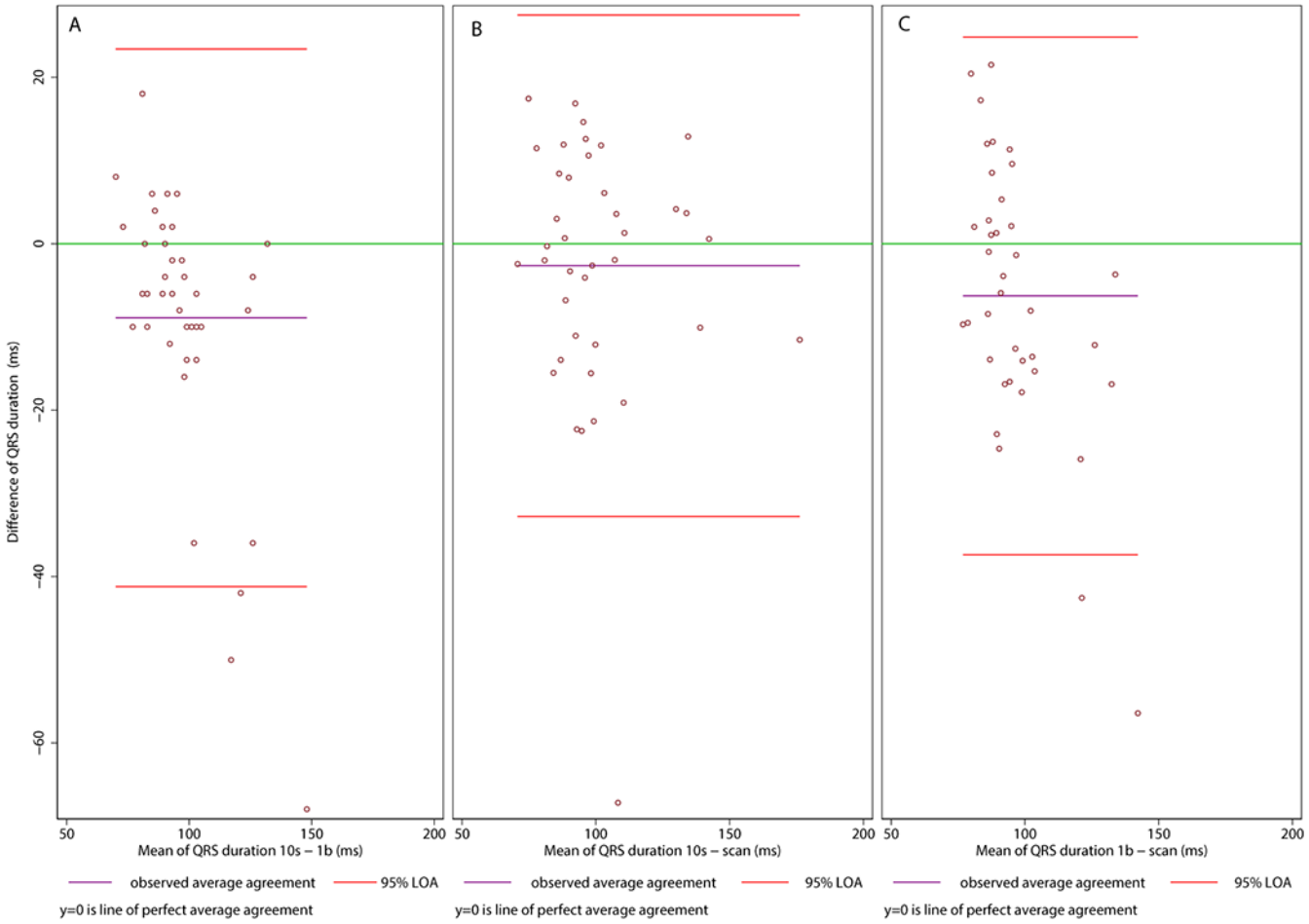

Figure 7.

Bland-Altman plots demonstrating agreement of QRS duration across 3 types of median or representative beats comprised of digitally recorded, simultaneous ECG leads (10s), digitally recorded, asynchronous ECG leads (1b), and digitized, asynchronous ECG leads (scan). The scatterplot presents paired differences (Y-axis), plotted against pair-wise means (X-axis). The reference line indicates the perfect average agreement, Y = 0. The central green line indicates the mean difference between the two measurements, or mean bias. Upper and lower lines represent the mean ± 2 standard deviations, or 95% limits of agreement. A. Agreement of (10s) digitally recorded, simultaneous ECG leads and (1b) digitally recorded, asynchronous ECG leads. B. Agreement of (10s) digitally recorded, simultaneous ECG leads and (scan) digitized, asynchronous ECG leads. C. Agreement of (1b) digitally recorded, asynchronous ECG leads and (scan) digitized, asynchronous ECG leads.

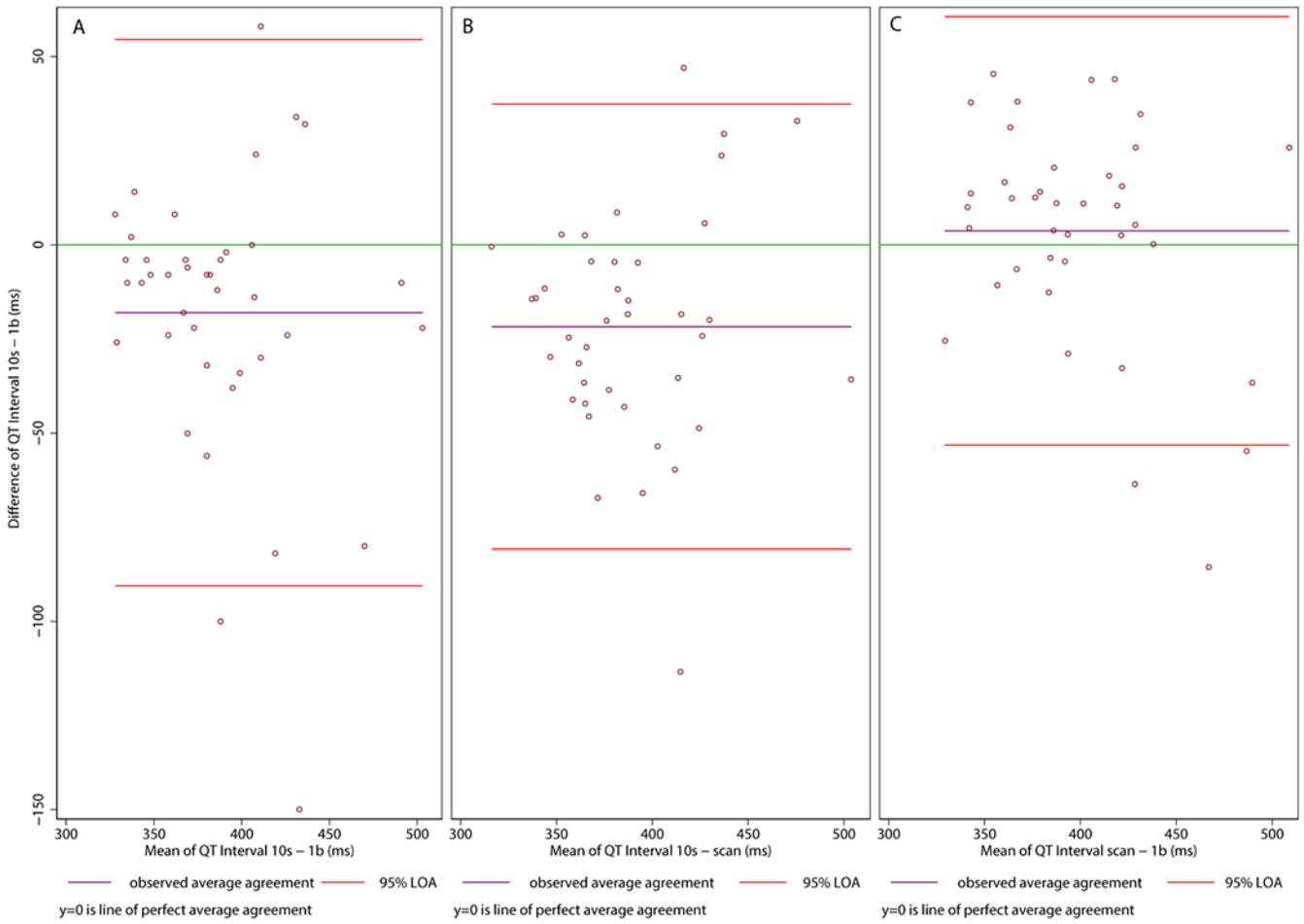

Figure 8.

Bland-Altman plots demonstrating agreement of QT interval. See Figure 7 legend for the details.

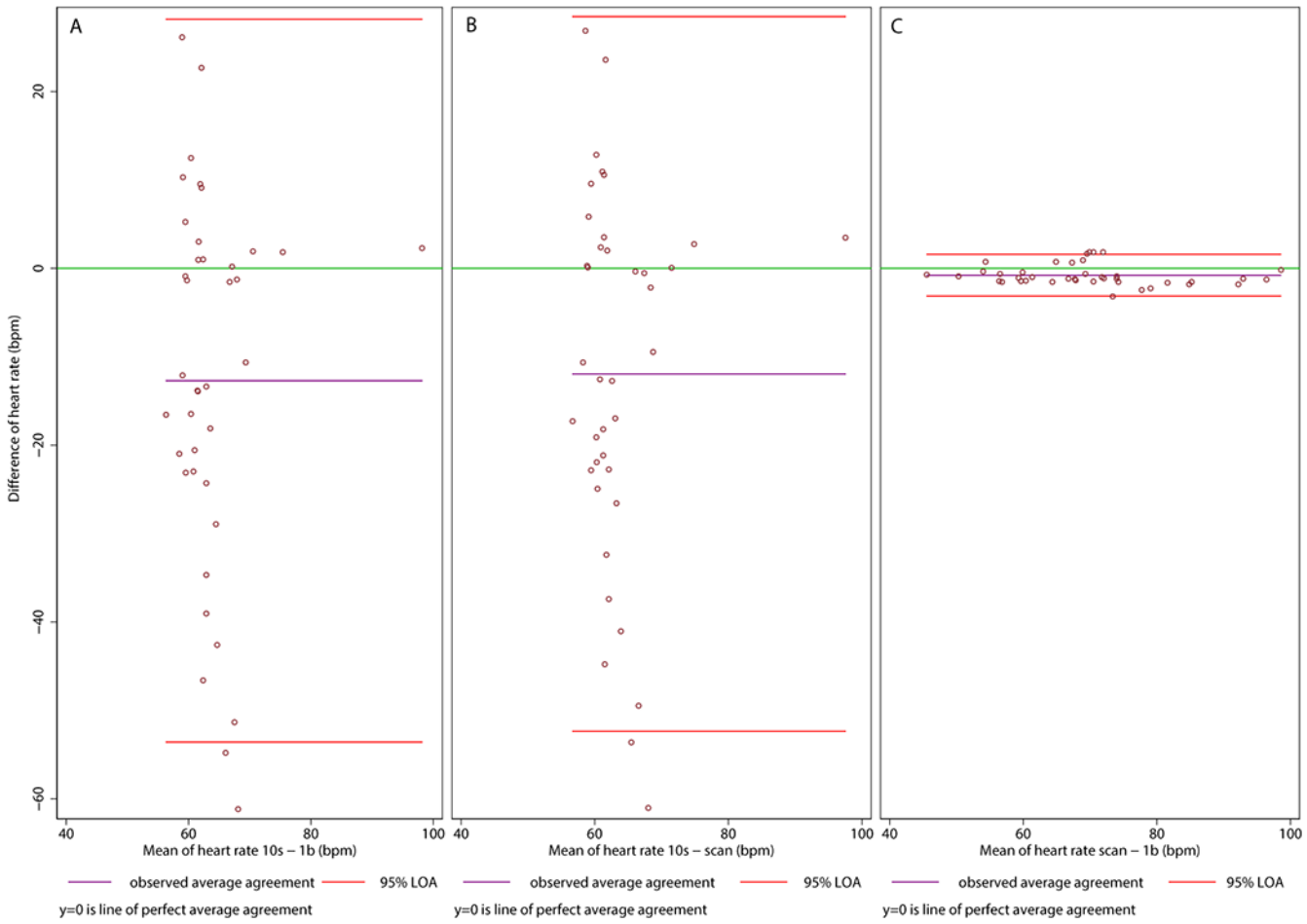

Figure 9.

Bland-Altman plots demonstrating agreement of heart rate. See Figure 7 legend for the details.

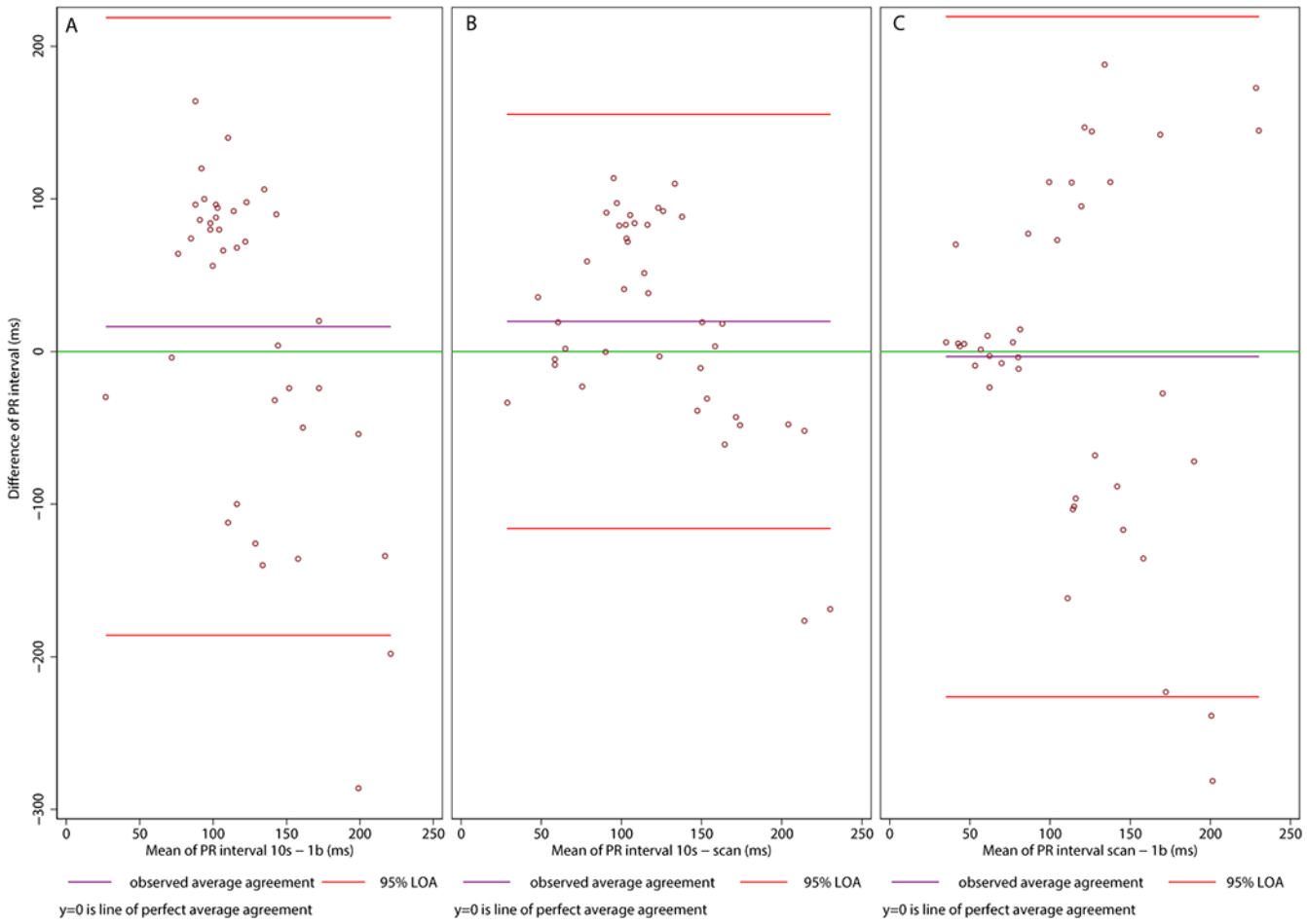

Figure 10.

Bland-Altman plots demonstrating agreement of PR interval. See Figure 7 legend for the details.

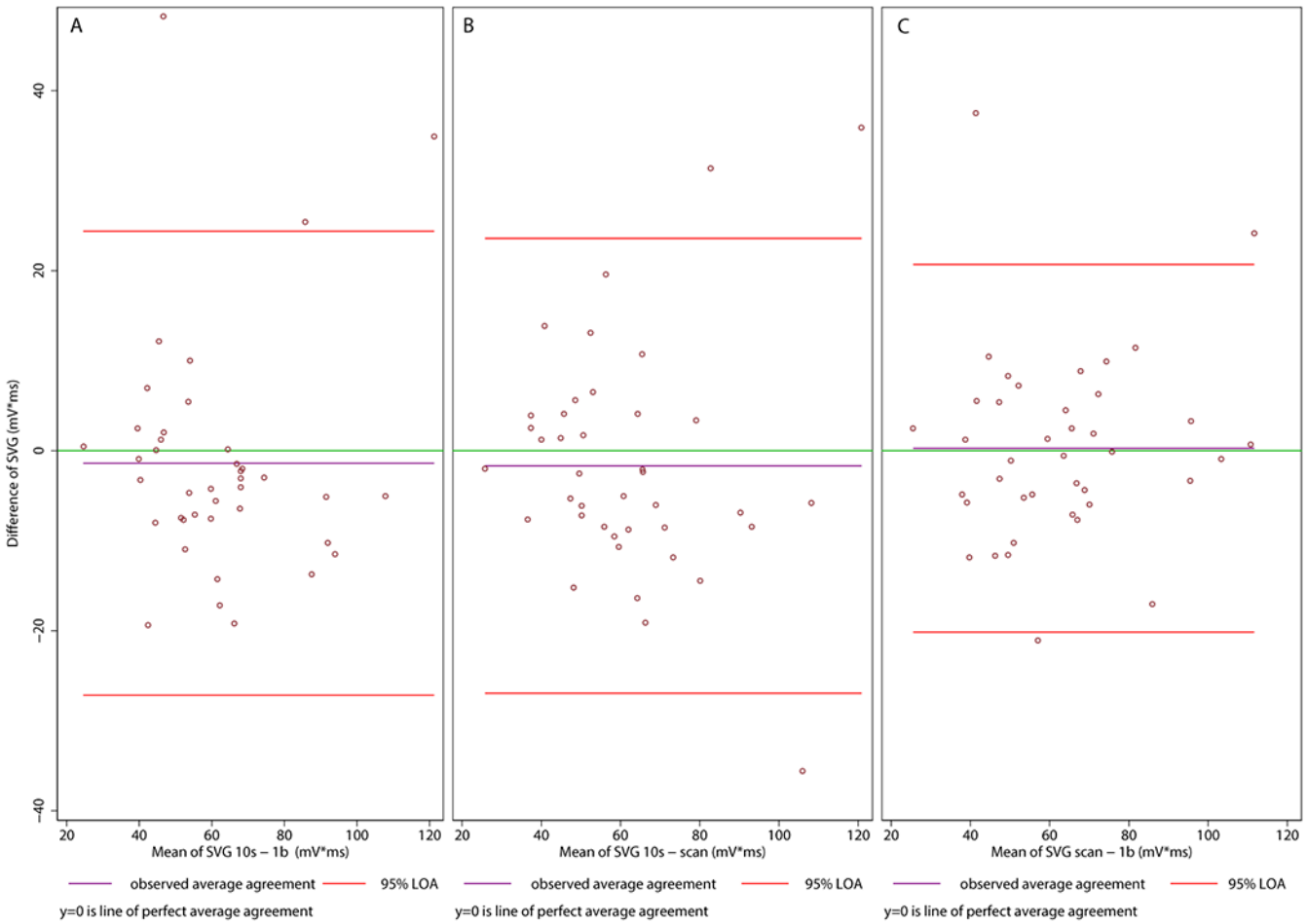

Figure 11.

Bland-Altman plots demonstrating agreement of Spatial Ventricular Gradient (SVG). See Figure 7 legend for the details.

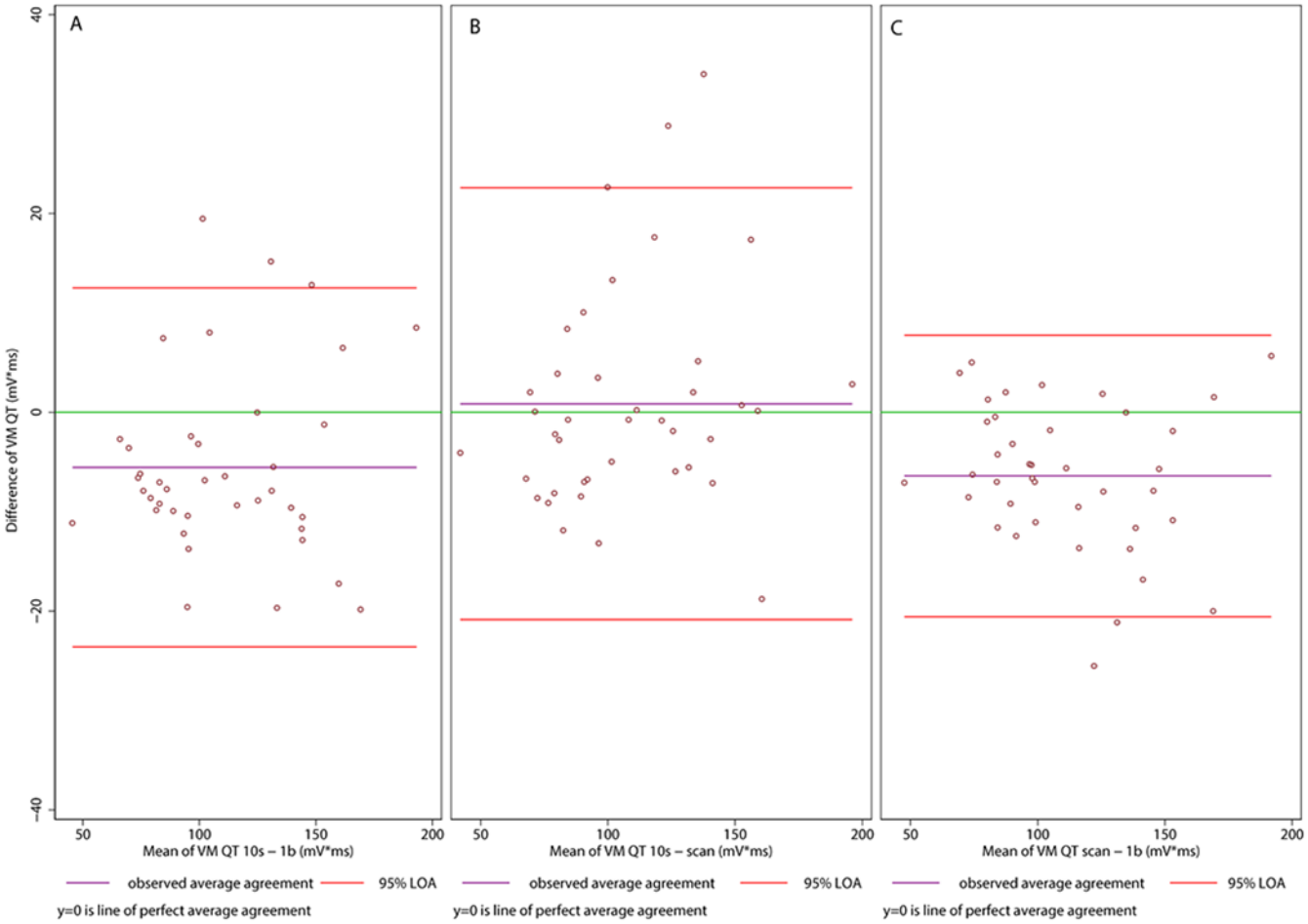

Figure 12.

Bland-Altman plots demonstrating agreement of Vector Magnitude QT integral ($VMQT_i$). See Figure 7 legend for the details.

Table 1.

Input and output in each step of the complex task of digitizing an ECG scan.

Process steps	Input	Output
Pre-processing & Digitization	Color image	Scalar or tensor data
Detection	Color image	Binary image
Extraction	Binary image	Scalar or tensor data

Table 2.

Study population characteristics

	All (n=230)	Development (n=150)	Validation (n=80)
Age(mean±SD), yrs	29.6±14.5	29.7±15.0	29.5±13.9
Female, n(%)	57(24.8)	40(26.7)	17(21.3)
White, %	203(88.3)	134(89.3)	69(86.3)
Body mass index(mean±SD), kg/m^2	29.0±8.0	28.8±7.8	29.2±8.2
Cardiovascular disease, n(%)	120(52.3)	80(53.3)	40(50.0)

Table 3.

Root mean squared error (RMSE) for ECG leads

ECG lead	RMSE (mean ± SD) μV
Lead I	27.6 ± 11.8
Lead II	28.3 ± 12.2
Lead III	27.9 ± 11.5
Lead aVR	29.2 ± 12.5
Lead aVL	28.3 ± 12.2
Lead aVF	27.7 ± 12.7
Lead V1	31.5 ± 11.4
Lead V2	31.8 ± 10.8
Lead V3	31.7 ±10.9
Lead V4	30.3 ± 12.1
Lead V5	30.3 ± 12.0
Lead V6	30.6 ± 11.6

Table 4.

Agreement of ECG and VCG GEH measurements on digitally recorded and digitized ECG signal, in 3 types of beats.

Measurement N=40	ECG 10s mean(SD)	ECG 1b mean(SD)	ECG scan mean(SD)	Bias 10s-1b (95%LOA)	Bias 1b-scan (95%LOA)	Bias 10s-scan (95%LOA)	Precision 10s-1b, %	Precision 1b-scan,%	Precision 10s-scan,%	ICC 10s-1b	ICC 1b-scan	ICC 10s-scan	Lin ρ_c (95%CI) 10s – 1b	Lin ρ_c (95%CI) 1b-scan	Lin ρ_c (95%CI) 10s-scan
Heart rate, bpm	57.5(12.4)	70.2(12.5)	69.4(12.3)	12.7(−53.6; 28.1)	0.8(−3.1-1.6)	11.9(−28.5; 52.3)	81.0	98.8	82.3	0.582	0.998	0.576	−0.27(−0.46-(−0.05))	0.99(0.99-1.00)	−0.27(−0.47-(−0.05))
PR interval, ms	131(41.3)	115(83.4)	112(72.2)	16.4(−186; 219)	3.4(−226; 219)	19.7(−155; 116)	87.8	97.7	73.9	0.449	0.119	0.526	−0.22(−0.44-0.02)	−0.06(−0.39-0.25)	0.29(0.04-0.51)
QRS duration, ms	93(12.9)	102(23.2)	99.2(21.5)	8.9(−41.2; 23.4)	2.6(−32.8; 27.5)	6.3(−24.8; 37.4)	90.3	97.2	92.8	0.841	0.868	0.810	0.55(0.38-0.69)	0.76(0.59-0.84)	0.56(0.37-0.71)
QT interval, ms	378(42.4)	396(49.3)	400(39.7)	18(−90.5; 54.5)	3.8(−53.2; 60.6)	21.7(−37.3; 80.8)	95.6	99.1	94.9	0.812	0.890	0.845	0.63(0.42-0.77)	0.79(0.64-0.88)	0.64(0.44-0.76)
QTc, ms	371(74)	425(53)	427(46)	−54.3(−202; 93.9)	2.0(−59; 63)	56.3(−88; 201)	87.4	99.6	87.7	0.489	0.896	0.464	0.23(0.01-0.05)	0.80(0.66-0.89)	0.19(−0.01-0.37)
Peak QRS-Tangle,°	47.4(40.1)	41.0(36.1)	48.0(37.3)	6.4(−60.0; 72.9)	7.0(−42.5; 56.6)	0.6(−69.5; 70.7)	64.6	60.6	95.2	0.757	0.866	0.730	0.60(0.436-0.76)	0.75(0.58-0.86)	0.57(0.32-0.75)
Area QRS-Tangle,°	66.4(37.4)	67.8(35.9)	65.0(37.2)	1.4(−33.2; 30.3)	2.8(−39.0; 33.3)	1.4(−37.0; 34.3)	94.8	90.8	94.5	0.949	0.932	0.937	0.90(0.82-0.95)	0.87(0.77-0.93)	0.88(0.79-0.94)
Peak SVG azimuth,°	11.5(4; 19)	−8.4(−20; 4)	−5.7(−22; 10)	19.4(−57.9; 96.6)	2.3(−87.5; 92.2)	17.0(−121; 86.6)	90.3	98.1	90.9	0.706	0.715	0.504	0.48(0.24-0.67)	0.55(0.30-0.73)	0.30(0.03-0.53)
Area SVG azimuth,°	−4(−10; 2.5)	−8(−13; −2)	−8(−16; −1)	3.6(−20.5; 27.7)	0.8(−26.8; 25.2)	4.4(−30.6; 21.9)	97.7	99.4	96.9	0.965	0.966	0.965	0.93(0.87-0.96)	0.93(0.87-0.96)	0.92(0.86-0.96)
Peak SVG elevation,°	48.6(29.0)	45.1(29.0)	46.6(34.7)	3.5(−30.7; 37.6)	1.5(−37.1; 40.1)	2.0(−41.2; 37.2)	95.2	97.7	97.2	0.901	0.903	0.900	0.81(0.68-0.90)	0.81(0.68-0.89)	0.80(0.67-0.89)
Area SVG elevation,°	66.2(19.7)	51.8(24.1)	54.3(24.5)	14.5(−10.0; 43.0)	2.5(−7.9; 13.0)	11.9(−40.6; 16.8)	81.7	96.8	85.3	0.887	0.988	0.890	0.64(0.47-0.77)	0.97(0.95-0.98)	0.68(0.51-0.80)
Peak SVG_{mag},mV	1.89(0.49)	1.85(0.40)	1.54(0.41)	0.04(−0.67; 0.76)	0.31(−0.83; 0.22)	0.35(−1.01; 0.31)	97.3	75.6	75.7	0.813	0.877	0.848	0.67(0.46-0.80)	0.60(0.43-0.74)	0.56(0.37-0.70)
SVG,mV*ms	61.1(21.6)	62.5(20.8)	62.8(21.8)	1.4(−27.2; 24.4)	0.3(−20.2; 20.7)	1.7(−23.6; 26.9)	97.4	99.5	96.9	0.894	0.937	0.903	0.81(0.66-0.89)	0.88(0.79-0.93)	0.82(0.69-0.90)
VM QTi, mV*ms	108(34)	114(33)	107(32)	5.5(−23.6; 12.5)	6.4(−20.6; 7.8)	0.9(−22.6; 20.9)	93.4	92.0	99.0	0.981	0.988	0.972	0.95(0.91-0.97)	0.96(0.92-0.98)	0.94(0.90-0.97)
SAIQRST, mV*ms	164(52)	173(49)	160(48)	8.4(−42.5; 25.6)	12.3(−36.6; 12.1)	3.9(−43.6; 35.9)	93.2	89.8	96.8	0.971	0.984	0.959	0.93(0.87-0.96)	0.94(0.89-0.96)	0.92(0.85-0.95)
Peak QRS_{mag}, mV	1.53(0.45)	1.53(0.32)	1.26(0.34)	0.17(−0.47; 0.81)	0.27(−0.70; 0.17)	0.40(−0.33; 1.12)	86.2	71.5	63.3	0.810	0.876	0.752	0.58(0.01-0.87)	0.59(0.41-0.72)	0.39(−0.12-0.73)
Peak T_{mag}, mV	0.50(0.16)	0.43(0.14)	0.42(0.16)	0.06(−0.06; 0.19)	0.03(−0.08; 0.02)	0.09(−0.20; 0.29)	82.3	90.9	76.3	0.961	0.994	0.974	0.82(0.47-0.95)	0.97(0.95-0.98)	0.76(0.41-0.92)

Measurement N=40	ECG 10s mean(SD)	ECG 1b mean(SD)	ECG scan mean(SD)	Bias 10s-1b (95%LOA)	Bias 1b-scan (95%LOA)	Bias 10s-scan (95%LOA)	Precision 10s-1b, %	Precision 1b-scan,%	Precision 10s-scan,%	ICC 10s-1b	ICC 1b-scan	ICC 10s-scan	Lin ρ_c (95%CI) 10s – 1b	Lin ρ_c (95%CI) 1b-scan	Lin ρ_c (95%CI) 10s-scan
VM QRSi, mVms	50.4(34.7)	50.1(34.4)	35.6(20.0)	0.25(−6.89; 7.41)	0.93(−12.7; 10.9)	1.0(−11.3; 13.3)	99.0	96.3	96.0	0.997	0.976	0.992	0.99(0.97-1.00)	0.95(0.91-0.97)	0.98(0.92-0.997)
VM Ti, mVms	58.7(25.7)	40.8(14.1)	41.1(14.1)	17.9(−13.9; 49.6)	0.90(−9.7; 7.7)	17.5(−46.4; 11.3)	39.4	96.3	40.6	0.904	0.987	0.941	0.49(0.08-0.76)	0.97(0.95-0.99)	0.53(0.14-0.78)

LOA=limits of agreement. Comparison 10s-1b is between time-coherent median beat constructed using 10-second digitally recorded data and representative asynchronous digitally recorded beat. Comparison 1b-scan is between representative asynchronous digitally recorded beat and the same beat obtained from scanned and digitized paper-ECG. Gray boxes indicate a statistically significant (P<0.001) Bradley-Blackwood F-test, implying that the reported results of the Bland-Altman analysis are biased. Circular variables are summarized as mean (95% confidence interval). Mag=magnitude; VM=vector magnitude; QRSi=QRS integral (area); Ti=T-wave integral (area).